

ASTROMER

A transformer-based embedding for the representation of light curves

C. Donoso-Oliva^{1,3,4}, I. Becker^{2,4,5}, P. Protopapas^{3,5}, G. Cabrera-Vives^{1,4}, Vishnu M.⁵, and Harsh Vardhan⁵

¹ Department of Computer Science, Universidad de Concepcion, Concepcion, 4070386, Chile

² Department of Computer Science, Pontificia Universidad Catolica de Chile, Macul, Santiago 7820436, Chile

³ Inst. for Applied Computational Science, Harvard University, Cambridge, MA 02138, USA

⁴ Millennium Institute of Astrophysics (MAS), Nuncio Monsenor Sotero Sanz 100, Providencia, Santiago, Chile

⁵ Univ.AI, Singapore, 050531, Singapore

Received x xxx xxxx / Accepted x xxx xxxx

ABSTRACT

Taking inspiration from natural language embeddings, we present ASTROMER, a transformer-based model to create representations of light curves. ASTROMER was trained on millions of MACHO R-band samples, and it can be easily fine-tuned to match specific domains associated with downstream tasks. As an example, this paper shows the benefits of using pre-trained representations to classify variable stars. In addition, we provide a python library including all functionalities employed in this work. Our library includes the pre-trained models that can be used to enhance the performance of deep learning models, decreasing computational resources while achieving state-of-the-art results.

Key words. Methods: statistical, Techniques: photometric, Stars: variables

1. Introduction

Over the past decades, efforts have been made to develop machine learning tools to analyze and discover variable phenomena in the sky. These tools will face a challenge, with the construction of the new generation of telescopes, which will generate substantially more data than the old generation (Kremer et al. 2017). Moreover, the observations will be deeper and more precise than ever.

With the upcoming telescopes such as the Vera C. Rubin Observatory (Ivezić et al. 2019), periodic observations of the a significant portion of the sky every few days will become the norm. They will produce light curves for all the objects in the observed fields.

Traditional machine learning (TML) methods rely on features to explore the variable behavior of light curves. They are based on quantities such as amplitude, period, color information, among others (Sánchez-Sáez et al. 2021). The expected volume of data will present a significant challenge to feature-based methods, if applied to every measured object.

Deep learning techniques have an advantage over TML as they do not need to pre-calculate features, extracting informative representations of the data automatically (LeCun et al. 2015). Also, deep learning methods leverage GPU parallelization, which accelerates the information extraction from the light curves.

In the last years, some of these methods have been developed with promising results. Naul et al. (2018) presented a recurrent autoencoder to extract features from folded periodical light curves. After training, the authors fitted a

Random Forest classifier on the embedded space, outperforming models trained on pre-defined features. This model was one of the first approaches in astronomy that used unlabeled light curves to extract characteristics from an unsupervised deep learning model. A similar idea was proposed a year later, by Tsang & Schultz (2019) used an autoencoder not only for classification but also for novelty detection. These approaches remain supervised, which is problematic for training on small datasets (Charnock & Moss (2017)).

Self-supervised models are ideal to overcome the limitations of labeled datasets, as they can generate the target values automatically without human-generated labels (Liu et al. (2021)). Most of these methods learn representations by solving auxiliary tasks which do not require any label, such as infilling of time series. The learned representations can be used downstream to solve other tasks, such as classification of variable stars or regression of physical parameters such as temperature or redshift. This learning scheme has achieved impressive results in Natural language processing (NLP), with Bidirectional Encoder Representations from Transformers (BERT, Devlin et al. (2018)) being one of the most notable examples. BERT-like models learn to extract contextual representations using two auxiliary tasks from a dataset of raw text. In this stage, known as pre-training, the model learns a general representation of the data, without being specific to any particular task. This process is the most resource-intensive part that usually takes weeks to complete, as the models as well as the datasets are large. After this stage is complete, the model only needs a few hours of further training to adjust the weights to a more specific domain, in a stage known as fine-tuning. Once finalized, BERT is used as the initial stage of a new model. Since the evaluation is much faster and ef-

Send offprint requests to: Cristobal Donoso-Oliva, e-mail: cridonoso@inf.udec.cl

ficient than the training of the weights in the pre-training stage. This scheme enables BERT-based models to achieve state-of-art performance.

The main components of BERT are the self-attention layers (Vaswani et al. (2017)), that codify similarities between words in the input sentence. These layers can be computed efficiently in parallel, in contrast to the sequential behavior of recurrent neural networks.

Following the advances on NLP to treat sequential data, representation learning and self-supervised training strategies, we present ASTROMER, a self-supervised model to extract a universal representation of astronomical light curves.

Our contributions can be summarized as follows:

1. We introduce ASTROMER, a self-supervised model that creates light curves representations taking advantage of the massive unlabeled volume of astronomical data.
2. ASTROMER representations speed up the training of downstream models such as classifiers of variable stars.
3. We empirically demonstrate the benefits of using pre-trained representations when training on small datasets. Using less than 100 samples per class, we significantly overcome an LSTM trained on light curves.
4. We provide a python library that includes pre-trained models and everything necessary to fine-tune and obtain domain specific embeddings.
5. Sharing pre-trained models by the community to save computational resources, decreasing CO2 emissions while improving the performance of automatic learning models.

Furthermore, we aim to create different versions of ASTROMER, just as BERT has many variations depending on the target (Polignano et al. (2019), Liu et al. (2019), de Vries et al. (2019), Moradshahi et al. (2019), Masala et al. (2020), Vunikili et al. (2020)).

2. Problem Statement

Let $X \in \mathbb{R}^{L \times d_x}$ be a single-band light curve where d_x is the number of features with L observations over time. In this case, every observation consists of $d_x = 2$ two descriptors: the magnitude and the Modified Julian Date (MJD), where the observations occur. Naturally, the number of observations and their MJD sampling times vary between different stars, and it strongly depends on the survey science goals. The maximum number of points in the light curves remains fixed even if some of them are shorter than L , in which case we perform padding and masking.

The main objective, is to train a model $f(X, \mathcal{D}_A, \theta)$ on a massive set of light curves \mathcal{D}_A from a given survey A . In particular, we propose to use learned representations of a transformer-based encoder to create embeddings $Z \in \mathbb{R}^{L \times d_k}$ representing the objects' variability in d_k -dimensional space. We can fine-tune the model's weights to adapt to other surveys and use it to solve downstream tasks, such as classification or regression.

3. Methods

In this section, we describe the main components of ASTROMER, which belong to the Transformer neural network proposed by Vaswani et al. (2017). In particular, we

focus on two processes: the self-attention block and the positional encoding. Both methods are necessary to capture relationships and encode light curves.

3.1. Self-Attention Block

Vaswani et al. (2017) introduced the self-attention mechanism as an alternative to the classical attention technique based on Recurrent Neural Networks (RNNs). The idea is to quantify relationships between observations without conditioning the operations to follow a sequential order. Thus, unlike RNNs, self-attention blocks can be executed in parallel, being more efficient and faster to train.

An attention block consist of multiple self-attention heads, that compute the similarities of every input within the sequence to each other.

Intuitively, every head focuses on a different input aspect, adding more information to the final representation. Inside every head, the input is transformed into three vectors corresponding to the (Q)uery, the (K)ey, and the (V)alue. Given a light curve sample $X \in \mathbb{R}^{L \times d_x}$ and the weights of the i -th head ($W_i^q, W_i^k, W_i^v \in \mathbb{R}^{d_x \times d_k}$), we compute the vectors as follows,

$$Q_i = XW_i^q, \quad K_i = XW_i^k, \quad \text{and} \quad V_i = XW_i^v. \quad (1)$$

In equation 1, the weights have zero mean and unit variance by definition. Therefore, we use Q_i the query and K_i the key vectors to calculate similarities and scale V_i the projected input values as follows,

$$Z_i = \text{softmax} \left(\frac{Q_i K_i^T}{\sqrt{d_k}} \right) V_i, \quad (2)$$

where d_k is a hyper-parameter specifying the embedding size of each self-attention head. The normalization factor $\sqrt{d_k}$ in the denominator scales the variance of the product to 1 while the softmax bounds the values to represent a multinomial probability distribution. The final attention vector is the normalized concatenation of Z_i the output from every i -th head in the block. Figure 1 illustrates the self-attention block. In this case, the size of Z the final attention vector is proportional to the number of heads.

3.2. Positional Encoding

Unlike recurrence-based models, the self-attention block cannot distinguish relative positions in the input sequence. Thus, any re-ordering of the input produces the same attention vectors. To incorporate time into the self-attention mechanism, Transformers use a positional encoder (PE; Vaswani et al. (2017)). In the original implementation, the PE assumes regularity of the text-based input, where every pair of consecutive words is equally-spaced. In contrast, observation times in a light curve are unevenly sampled for every object. Therefore, we will use the times directly to compute a PE.

In this implementation, the PE consist of trigonometric functions that codify t_l a single time from the l -th observation t_l at different w_i frequencies,

$$PE_{2i,t_l} = \sin(t_l \cdot \omega_i), \quad PE_{2i+1,t_l} = \cos(t_l \cdot \omega_i). \quad (3)$$

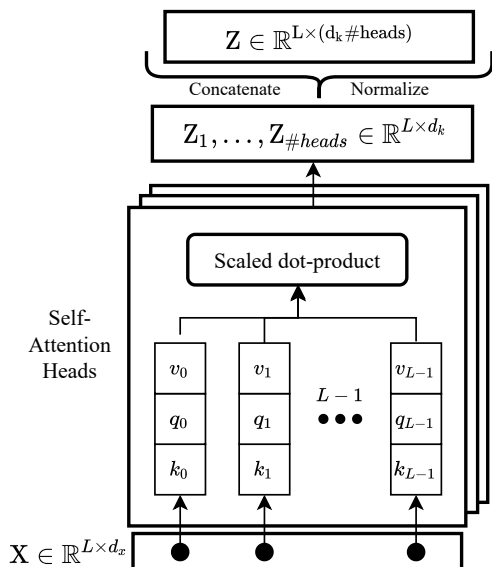


Fig. 1. Self-attention block diagram. Each observation vector $\mathbf{x}_i \in X$ (denoted by solid circles) is projected into three vectors: (k)ey, (q)uery, and (v)alue. Then their similarities are computed by the scaled dot-product between vectors according to equation 2.

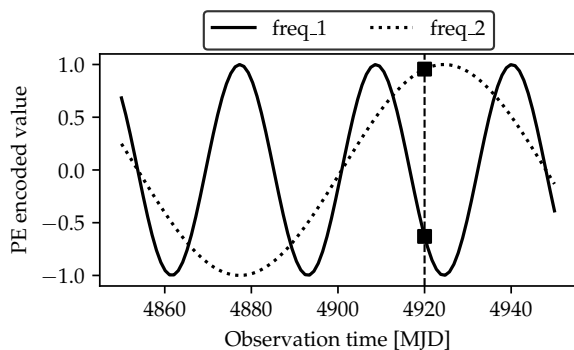


Fig. 2. Example of two-frequencies positional encoding codifying the same observation time.

In Equation 3, $i \in [1, \dots, d_{pe}]$, where d_{pe} is the PE dimensionality and w_i the angular frequency defined as

$$\omega_i = \frac{1}{1000^{2i/d_{pe}}}. \quad (4)$$

Including more frequencies enables the model to capture patterns present at different time-scales. Figure 2 shows an example of two different frequencies receiving the same observation time, capturing different temporal patterns at different time scales.

In equation 4, the denominator controls the time-scales for the frequencies. We empirically defined the base to 1000 since the light curves do not reveal significant variations on the embedded space using larger values. Figure 3 shows an example of the resulting PE for a light curve sample (MACHO ID=F1_4175.3433).

For a light curve of length L , the positional encoding will be a matrix of dimensions $L \times d_{pe}$. This matrix is added to the input matrix X . It is essential to highlight that the PE

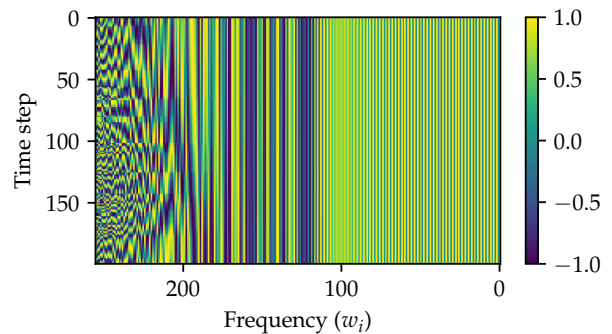


Fig. 3. Resulting positional embeded space from the F1_4175.3433 MACHO object.

dimensionality conditions the input size of the model as a function of the number of time scales d_{pe} . Thus, the larger this value, the greater the number of parameters used in the model's layers.

4. Proposed Solution

Here we introduce and describe ASTROMER, a transformed-based model for the automatic representation of light curves. We combine the recent advances in deep learning with the large volume of data in astronomy to create a self-supervised model able to produce stars embeddings. In particular, we take inspiration from the BERT language model (Devlin et al. (2018)), which uses masked self-attention to learn text representations.

Section 4.1 introduces a general overview of ASTROMER by describing the model's architecture. Then, Sections 4.2 and 4.3 present the fundamental mechanisms of the encoder and decoder modules to create embeddings. Finally, we explain the masked self-attention technique in Section 4.4, which is the backbone of the self-supervised training strategy that helps the model to understand the light curve domain.

4.1. Model Architecture

ASTROMER has an encoder-decoder architecture, as shown in Figure 4. All samples have a maximum of 200 observations, which can be modified if necessary. In this case, the number of frequencies in the PE conditions the input dimension, changing from 2 to 256. On top of the encoder, we use two self-attention blocks with four heads of 64 neurons each. The final representation is a collection of 200 vectors of size 256 describing the attention of every observation to each other. We use light curves representations to reconstruct the input magnitudes in the decoder. Although the decoder presented in Figure 4 is exclusive for training ASTROMER, we can use different decoding layers focusing on other downstream tasks.

4.2. Building representations

The first step in ASTROMER is the normalization of vectors. Here the sample mean of the light curve is subtracted to each observation within the 200-length window. Then, the PE is created as explained in Section 3.2. The dimen-

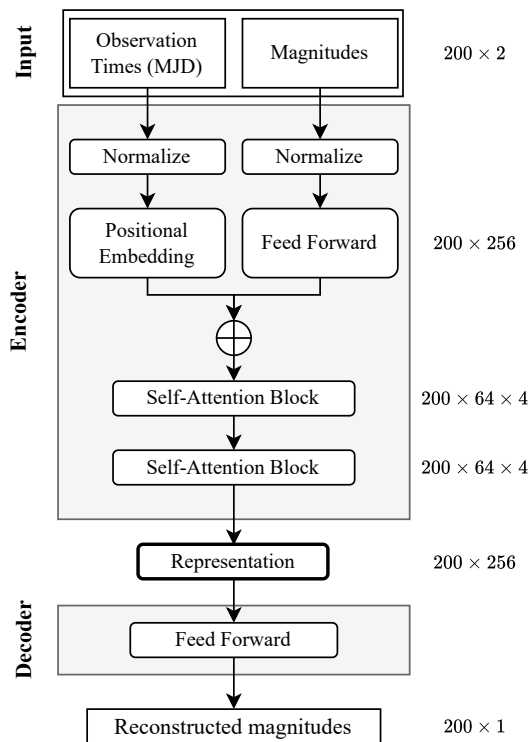


Fig. 4. ASTROMER architecture

sion of the PE (256) defines the number of frequencies we use to project times on different scales.

On the other hand, the magnitudes must be reshaped to match the PE dimensionality. In this model, a time-distributed dense layer projects each magnitude to a 256-dimensional space. Finally, the PE and the transformed magnitudes are added to form the input of the attention block.

Self-attention blocks receive transformations of light curves that include temporal and brightness information combined on the same vector. Inside the encoder, we use two layers of self-attention blocks with four heads each. Stacking layers allows the model to achieve higher levels of abstraction when computing the attention vectors, as the second block uses as input the representation learned in the first block. Finally, the output of the last self-attention block is used to represent the light curve. Notice that no single 256-dim vector describes the entire sample but rather a collection of them.

4.3. Defining a proper decoder

The decoder is essential to adjust the encoder weights. The output conditions the purpose of the embedded representation. In this case, we use a regressor decoder to reconstruct the magnitudes. It corresponds to a dense layer transforming each 256-dimensional vector to the desired output dimension. The reconstruction of the entire light curve does not guarantee the creation of useful representations. To include semantic information in the embeddings, we apply the self-supervised methodology used in Devlin et al. (2018) to train the BERT text model. Their methodology is based on masked self-attention to learn syntactic, semantics, and contextual information. We hypothesize that using

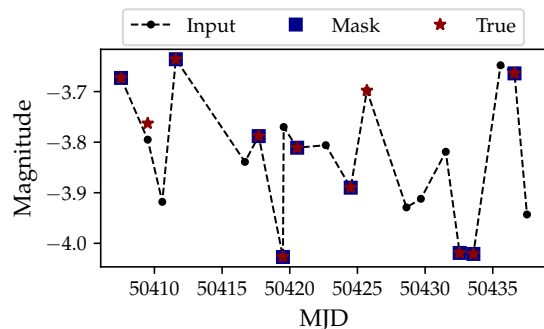


Fig. 5. 20 observations sampled from the F1_4175.3433 MA-CHO object after masking. Black circles represent the input of the model. Masked values (blue squares) are hidden from the self-attention blocks, which are not used to reconstruct the input magnitudes. Red stars refer to the valid values (target). Notice that 20% of the masked observations are assigned a random value. That is why the point close to 50410 MJD does not match the model's input. Similarly, 20% of the masks are removed, keeping the original value, as shown in the point next to the 50425 MJD.

the same technique can help the model better understand the astronomical domain. In the following Section 4.4, we explain how masked self-attention works.

4.4. Masked self-attention

The masked self-attention is a two-step process. First, 50% of random observations are selected to be reconstructed. Then, a 20% of the 100% masked values is replaced with random magnitudes and another 20% with the correct values. The remaining 60% is kept masked to be excluded from the final attention vector. Figure 5 shows an example of the resulting input after the masking process, where red stars refer to the true values to be reconstructed. The input observations, denoted by black circles joined by a dotted line, form the representation used to decode the entire example. In contrast, blue squares symbolize the masked values removed from the final representation. Intuitively, the mask allows the model to capture contextual information. If used without random replacements, the model can learn that every time the mask token appears it is a correct value. Similarly, if the correct values are not reintroduced, the model can assume that all unmasked values are wrong.

5. Data description

This section describes the data involved in the pre-training and fine-tuning of the ASTROMER model. Every light curve contains magnitudes and observation times in Modified Julian Date (MJD).

ASTROMER takes advantage of a massive set of light curves, not necessarily labeled. However, to evaluate a downstream task (i.e., classification), we use catalogs of variable stars with their corresponding labels. This work simulates the science case of having a small subset of labeled samples and employs them to fine-tune the model even when the class information is unnecessary.

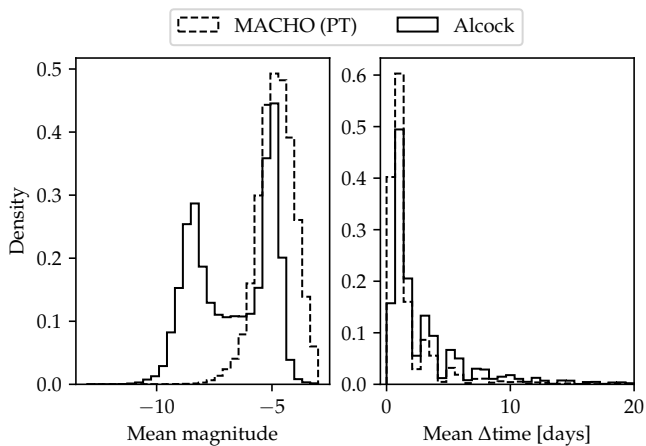


Fig. 6. Comparison between Alcock’s catalog and MACHO unlabeled dataset. [Top] Distribution of sampling time differences. [Bottom] Mean magnitudes distribution.

5.1. Unlabeled dataset

R-band light curves of the MACHO survey (Alcock et al. (2000)) were collected from the Galactic Bulge (Fields 1 and 10), and the Large Magellanic Cloud (LMC, Fields 101-104). Given the nature of photometric observations, the observed flux of every star will exhibit some kind of variability, such as the intrinsic observational noise. As such, we cannot expect every star to be variable. Even though non-variable and noisy data can be helpful to regularise weights (Bishop (1995)), we discard some of the light curves that show white noise behavior (i.e., $|\text{Kurtosis}| > 10$, $|\text{Skewness}| > 1$, and $\text{Std} > 0.1$). Removing white noise samples avoids training on a dataset dominated by irrelevant information while keeping variable objects that might contain informative variability. After this filtering process, 1 529 386 light curves are left, with a cadence mean of 2.9 ± 17.3 days.

5.2. Labeled datasets

We employ Alcock’s catalog of variable stars (Alcock et al. (2003)) to fine-tune and evaluate the downstream task, which includes 20 894 variable objects from the MACHO survey. Table 2 shows the class distribution. This catalog contains objects from the Large Magellanic Cloud, and shares similar properties as the unlabeled dataset previously described (see Figure 6). The labels were updated to conform to modern classifications. In particular, we group the LPV classes into one category and remove the categories "RR Lyrae and GB blends" and "RRe". The former are excluded because of their small sample size, and the latter because RRe are not considered a sub-class on its own based on later studies (Catelan (2004)).

We also tested ASTROMER on the datasets OGLE-III (Udalski (2004)) and ATLAS Heinze et al. (2018) catalogs of variable stars. The OGLE-III data used was selected by Becker et al. (2020) and contains 358 288 labeled variable stars and correspond to I-band light curves with mean cadence of 3.8 ± 14.6 days. Table 3 shows its class distribution. The OGLE-III catalog is chosen because its observations are not captured in the same filter as MACHO but close to its wavelength range, as shown in Table 1.

Table 1. Surveys and the filters used in this work. Taken from Alcock et al. (1999), Udalski et al. (2015) and Tonry et al. (2018), respectively. In Szymański et al. (2011) is noted that OGLE-III and OGLE-IV don’t have the same I filters, exhibiting a wide transparency “wing” towards the infrared part of the spectrum. Although different, we use Udalski et al. (2015) numbers as a reference, as they are intended to show the approximate ranges of the filters.

Survey	Filter Name	$\lambda_{min} \text{ } \circ A$	$\lambda_{max} \text{ } \circ A$
MACHO	R	6300	7600
OGLE	I	7270	8750
ATLAS	orange	5620	8200

Table 2. Alcock’s catalog distribution.

Tag	Class Name	# of sources
Cep_0	Cepheid type I	1182
Cep_1	Cepheid type II	683
EC	Eclipsing binary	6824
LPV	Long period variable	3046
RRab	RR Lyrae type ab	7397
RRc	RR Lyrae type c	1762
Total		20 894

Table 3. Becker 2020 catalog distribution

Tag	Class Name	# of sources
EC	Eclipsing binary	6862
ED	Detached Binary	21 503
ESD	Semi-detached Binary	9475
Mira	Mira	6090
OSARG	Small-amplitude red giant	234 932
RRab	RRLyra type ab	25 943
RRc	RRLyra type c	7990
SRV	Semi-regular variable	34 835
cep	Cepheid	7836
dsct	Delta Scuti	2822
Total		358 288

Table 4. ATLAS catalog distribution

Tag	Class Name	# of sources
CB	Close Binaries	80 218
DB	Detached Binary	28 767
Mira	Mira	7370
Pulse	RR Lyrae, δ -Scuti, Cepheids	25 021
Total		141 376

The ATLAS dataset, published by Heinze et al. (2018) contains labeled and unclassified objects as well as a dubious class which amounts to roughly 10% actual variable stars and 90% instrumental noise, according to their estimates. From this dataset, 422 630 light curves are used, measured in the orange passband, as seen in Table 4, with a mean cadence of 4.7 ± 19.1 days. The reported classes are grouped to obtain labels similar to the other datasets. In particular, we group CBF and CBH into Close binaries and DBF and DBH into Detached binaries. We don’t use the remaining objects, as their labels are based on Fourier analysis and do not correspond exactly to astrophysical categories.

5.3. Preprocessing

Neural networks must work with tensors holding equal-length samples. It is not the case of light curves that differ on the number of measurements.

We divide each light curve in L observations windows to generate equal-length samples. Without enough measurements, we zero-pad on the sequences until complete L the maximum length. Notice L is a hyper-parameter of the model which for this experiments is set to 200.

Finally, we subtract the sample mean to each light curve independently. It implies both magnitude and time vectors have zero-mean. We do not scale samples by their standard deviation, either magnitudes or time. Scaling by time dispersion would lose some of the interpretability for the positional encoder. Standardizing magnitudes may lose amplitude-related information, important to discriminate between some classes.

6. Training Strategy

In the following sections, we describe the training strategy consisting of two separate steps: the pre-training and the fine-tuning. All the light curves are used during pre-training. However, we study the science case of having small target datasets to perform downstream tasks. To do this, we sample 20, 50, 100, and 500 objects per class from each labeled dataset, using them independently to fine-tune ASTROMER. The idea is to see the impact of the number of samples when adjusting pre-trained weights on a different survey. In a second scenario, we use all the light curves from each dataset to fine-tune.

6.1. Pre-training

The pre-training constitute the first stage of representation learning. It defines the preliminary data requirements, such as cadence and filter, that condition other target domains. In this case, we use the massive unlabeled dataset from the MACHO survey presented in Section 5.1.

ASTROMER weights are initialized using the Xavier uniform initializer (Glorot & Bengio (2010)). Training big models such as ASTROMER uses a large amount of hardware resources and computational time. Despite this, once the weights are adjusted, they can be shared, avoiding re-training ASTROMER from scratch.

The unlabeled dataset is split into 60%, 20%, and 20% for training, validation, and testing, respectively. As mentioned in Section 5.3, the light curves are split into windows of 200 consecutive observations, increasing the effective number of training samples to 6 201 030. An epoch is completed after training in all samples once, in batches of 5000. We used Adam (Kingma & Ba (2014)) with custom learning rate (Vaswani et al. (2017)) controlled by,

$$lrate = d_k^{-0.5} \cdot \min(step^{-0.5}, step \cdot warmup^{-1.5}), \quad (5)$$

where d_k is the model size, $step$ is the forward pass iteration, and $warmup = 4000$ handles the increasing and decreasing trends. The training performance is evaluated on the validation dataset. Early stopping is used to stop the training after 40 epochs without improving the validation loss. Once the training is finished, the weights corresponding to the lowest RMSE are saved.

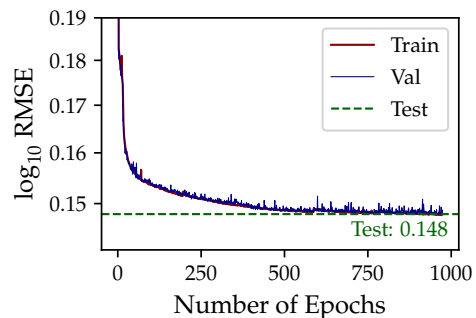


Fig. 7. Pre-training learning curves using MACHO unlabeled dataset.

Table 5. Fine-tuning training times. First column corresponds to the dataset used to fine-tune ASTROMER. As a reference, the first row shows the pre-training information from the MACHO unlabeled dataset. The total number of epochs for training is shown in Column 2. Column 3 and 4 are the time taken by a NVIDIA A100 and the lowest validation RMSE, respectively.

Dataset	# Epochs	# Time	RMSE
MACHO (PT)	970	9 days 17 hrs	0.15
MACHO	115	58 min	0.12
ATLAS	147	12 hrs 13 min	0.05
OGLE-III	244	1 day 3 hrs	0.03

Figure 7 shows the learning curves of the training process. The model reached the lowest validation RMSE close to epoch 1000¹, obtaining an error of 0.148 on the testing samples (dotted line).

6.2. Fine-tuning

After pre-training on the MACHO unlabeled dataset, the model has learned much of the variability patterns of the light curves. However, it is still necessary to incorporate downstream task-related information. In this work, we use catalogs of variable stars with different cadences and filters than the pre-training samples, as described in Section 5.2 to fine-tune the attention-based embedding.

The loss function and self-supervised strategy remain the same (i.e., RMSE and masked self-attention technique). The same hyper-parameters from the pre-training stage are used.

Table 5 shows the number of epochs and total time to fine-tune ASTROMER on each labeled dataset using all samples, comparing it to the pre-training stage. A significant difference to the pre-training time is evident. The fine-tuned models converge faster depending on their similarities and the number of samples. For instance, the model fine-tuned on OGLE-III light curves takes more time than the one trained on the MACHO labeled dataset. This is principally due to the survey differences and the number of samples that allow the model to get much lower RMSE than the MACHO labeled dataset. At the same time, similar behavior is observed on the ATLAS finetuning, where the training time is less than OGLE-III but greater than labeled MACHO.

Finally, the weights are saved to compute light curves representations that form the input to the downstream

¹ ~ 10 days training on a Nvidia A100 GPU

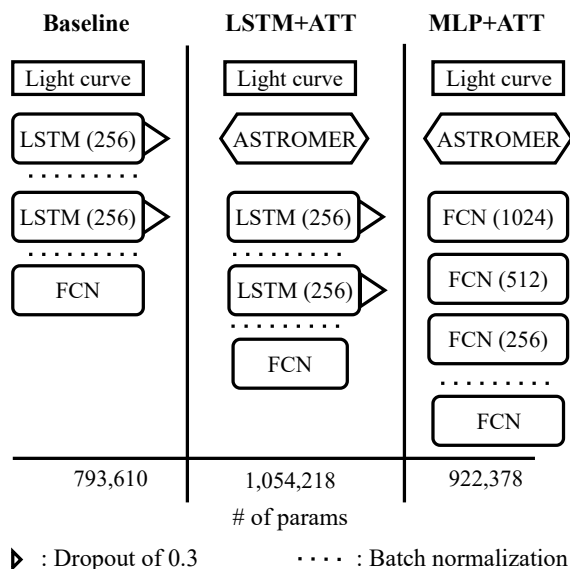


Fig. 8. Classifiers used to evaluate the effect of ASTROMER representations. Models with the +ATT tag refer to models trained on attention vectors. In contrast, the Baseline uses only the light curves for training.

models. In this case, we use ASTROMER to solve the classification of variable stars.

7. Specific Task: Classification

ASTROMER is designed as a general embedding that can be fine-tuned to solve downstream tasks such as classification or regression. In this work, we cover the problem of classifying variable stars from different surveys. As explained at the beginning of this section, the model is fine-tuned and evaluated in classification performances on labeled sub-samples of 20, 50, 100, and 500 objects per class and the entire dataset.

To evaluate the benefits of using the ASTROMER embeddings as opposed to other deep learning approaches, we implemented a baseline model, which consists of an LSTM trained directly on light curves. Hereafter, we will refer to this LSTM model as the Baseline. In the case of embedding-based classifiers, ASTROMER is used as an encoder at the beginning of the network, as shown in Figure 8. Thus, creating light curves representations in-place (or not previously saved), which can be used by the following classifier layers. For small training sets, freezing the weights of ASTROMER allows to train a classifier without training a huge number of weights. The ASTROMER encoder can also be trained in tandem with the classification network, to better tune weights to solve a specific task, which can be seen as another fine-tuning step. The following experiments evaluate these two approaches, i.e., training and non-training of the encoder layer of ASTROMER.

To measure the classification performance, the F1 score is used, which is a harmonic mean of the precision and recall metrics. Cross-validation is used on three random partitions of 100 samples per class for testing, and an 80%/20% split of the rest for training and validation, respectively.

Figure 9 shows the scores obtained by the classifiers by (a) freezing the encoder and (b) training the encoder. In addition, a third case (c) is included where all the light

curves in the dataset were used to perform fine-tuning, but still evaluating the classification on the smaller subsets. As in experiment (b), the third column allows gradients to flow into the ASTROMER encoder while training the classifiers.

The results show that models trained on ASTROMER representations perform better than the Baseline in MACHO and OGLE across all the experiments. For ATLAS, the difference is smaller but not worse than the Baseline. In general, the LSTM trained on attention vectors performs better than the MLP. However, the MLP+ATT outperforms the Baseline and approaches the LSTM performance as the number of samples per class is increased, in all datasets.

Note that in (c), even fine-tuning with all the light curves, the score improvement is discrete compared to (b). On the other hand, no improvements can be seen in the classification metrics when training with less than 50 samples per class and optimizing the encoder layer of ASTROMER -i.e., columns (b) and (c) in Figure 9.

We evaluate the improved learning speed when using ASTROMER. The average validation loss versus the training time is shown in Figure 10. This corresponds to experiments using 500 samples per class, representing the largest dataset used in this setup. Models trained on ASTROMER representations take less than half of the time to converge than the Baseline. This behavior also extends to the number of epochs where the best Baseline model spends 207 ± 80 epochs for training, while the LSTM and MLP trained on attention vectors take 97 ± 38 and 94 ± 28 , respectively.

8. Discussion

The results show the benefits of using pre-trained models to create representations to aid the training of other downstream tasks, such as classification. ASTROMER only needs to be fine-tuned to extract helpful representations of the target domain. Indeed, it is not mandatory to train ASTROMER when classifying.

The differences with the Baseline are more significant when training on small datasets. As the number of samples increases, the attention-based classifiers continue to improve their scores. However, after 100 samples per class it is convenient to use ASTROMER as a trainable layer of the classifier networks. It is not recommended to train ASTROMER on small datasets because the number of labels is not enough to optimize a large number of parameters. The improvements of (c) against (b) are discrete, which implies that most of the extracted information comes from ASTROMER's pre-training.

While the LSTM uses its hidden state to capture long and short-term relations on the attention vectors over time, the MLP deals with their average, losing the explicit temporal information in the representation. Furthermore, the embeddings cannot capture the global context as they only store pairwise similarities. Thus, the averaged attention of the MLP turns into a global-context embedding when we propagate class-informed gradients in cases (b) and (c) of Figure 9. While the LSTM+ATT performance remains almost the same in all scenarios for all datasets, the metrics for the MLP+ATT improve significantly.

Deep learning models trained on labeled samples need large datasets to achieve competitive performances. When using 500 samples per class, the Baseline approaches the scores of models trained on pre-trained representations.

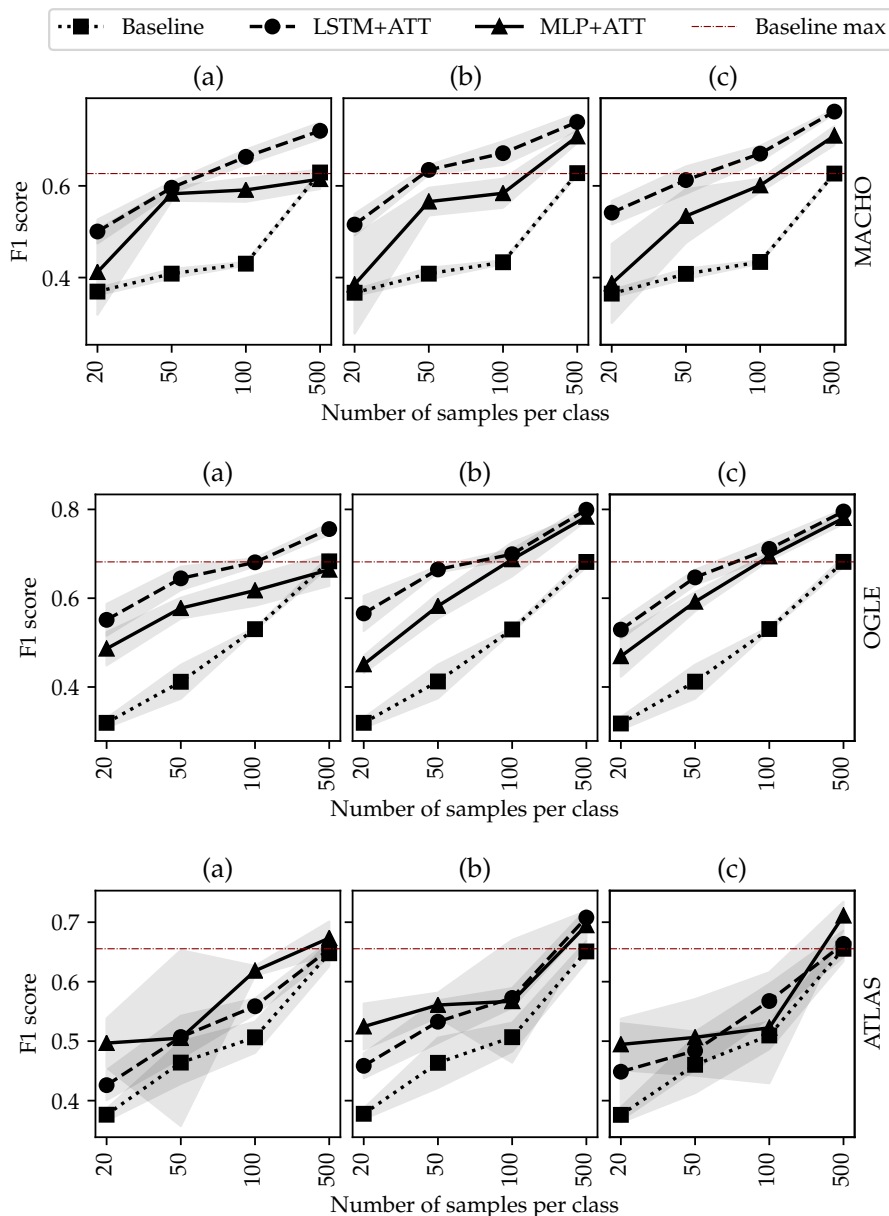


Fig. 9. F1 scores for an LSTM trained on light curves directly (Baseline) and models trained on ASTROMER representations (LSTM+ATT and MLP+ATT). Each row corresponds to the experiments on each survey, MACHO, OGLE and ATLAS, respectively. In (a), we fine-tune ASTROMER and optimize classifiers on smaller subsets of 20, 50, 100, and 500 samples per class. The weights of ASTROMER are kept frozen when classifying. However, in (b), we allow gradients to flow into ASTROMER. The third case (c) shows the results of fine-tuning with the entire set of light curves and classifying on smaller subsets, training ASTROMER simultaneously.

However, the classification metrics are still larger when using ASTROMER. Even though the main contribution of this work is to help training downstream models on small datasets, we achieved competitive results against Donoso-Oliva et al. (2021) using OGLE-III unfolded light curves (88.1% vs 88.0% ours). For Alcock’s catalog, We compare ASTROMER-based classifiers against the best (78.1% accuracy) single-band non-period informed model from Jamal & Bloom (2020). We achieved similar results, 78.2% and 76.7% classification accuracy for the LSTM+ATT and MLP+ATT, respectively.

Finally, thanks to the pre-training carried out by millions of light curves, models trained on ASTROMER repre-

sentations converge faster than the traditional deep learning models. We confirmed the advantages of separating the representation learning when solving a downstream task, such as classification. In Figure 10 we observed significant differences in the training times between ASTROMER-based classifiers and the Baseline. Shorter training times using shared pre-trained representations imply fewer resources, decreasing the time and energy consumption when training deep learning models (Dhar 2020).

9. Python Package

We provide a Python package of ASTROMER, which includes the pre-trained weights obtained in section 6.1 and

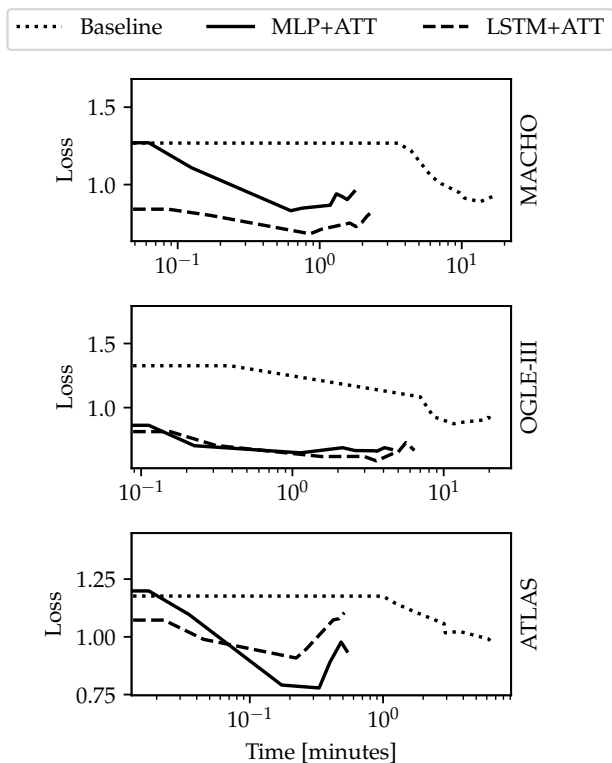


Fig. 10. Mean validation learning curves for the classifiers trained on 500 samples per class on each catalog. The loss is given by the categorical cross-entropy and remains the same for each classifier.

the fine-tuned variations on OGLE and ATLAS. More pre-trained models will be made available in the future, as well as giving the option for the users to upload their trained models. The stable version can be installed directly via the pip command:

```
pip install ASTROMER
```

The ASTROMER model is a class in the library and can be easily called as:

```
from ASTROMER import ASTROMER
model = ASTROMER()
```

The model can be loaded with pre-trained weights like `macho`, `atlas`, and `ogle`.

```
model = model.from_pretrained("macho")
```

To get embeddings of new light curves, we use the `encode` method of the class,

```
data = [ np.array([[5200, 0.3, 0.2],
                  [5300, 0.5, 0.1],
                  [5400, 0.2, 0.3]]),
        np.array([[4200, 0.3, 0.1],
                  [4300, 0.6, 0.3]]) ]
```

```
att_vectors = model.encode(data)
```

ASTROMER can be easily trained with tools inherited from the Keras' model class.

```
model.compile(optimizer='adam')
history = model.fit(data)
```

In addition to the library, we open project repositories² where data, tutorials, documentation, and contributions via issuing pull requests can be found. These contributions can be in the form of functionalities or pre-trained models.

10. Conclusion

We present ASTROMER, a single-band embedding for light curve representation. It is based on the BERT text model, which codifies samples in attention vectors via self-supervised learning taking advantage of the massive unlabeled volume of data. In this work, we pre-train ASTROMER on millions of R-band light curves from the MACHO survey.

ASTROMER can be fine-tuned on specific domain datasets to solve downstream tasks, such as classification or regression. Here, we use labeled catalogs from MACHO, OGLE-III, and ATLAS surveys to evaluate the effect of using embeddings on the classification of variable stars. By training a MLP and LSTM classifiers on self-attention vectors, we outperform a baseline LSTM recurrent neural network trained on light curves observations. We evaluated classification performances with 20, 50, 100, and 500 samples per class fine-tuned models, obtaining better F1 scores in all experiments. Additionally, we showed that the embeddings-based classifier achieved competitive scores against state-of-the-art solutions. In terms of training time, models trained on ASTROMER representations took less than half of the time of the baseline LSTM classifier to reach the lowest validation loss.

Our self-supervised approach only considers the reconstruction of magnitudes, not including other tasks, such as the next sentence prediction applied in BERT. As a result, the final representation may not satisfy other downstream tasks correctly. For instance, the consequences of losing global context information were evidenced on the difference between the MLP and LSTM classifier, both using attention vectors. In order to make embeddings more informative, we will explore adding new tasks during the pre-training and fine-tuning steps in future work.

Finally, we provided a python library including MACHO pre-training weights and fine-tuned models used in this work. Moreover, our library allows users to pre-train, fine-tune, and get embeddings on new single-band datasets. We aim to create a collaborative research environment where pre-trained ASTROMER weights can be shared, saving computational resources and improving state-of-the-art models.

Acknowledgements. This research was supported by the ANID Millennium Science Initiative ICN12 009, awarded to the Millennium Institute of Astrophysics; FONDECYT Initiation N° 11191130 (G.C.V.); the Patagón supercomputer of Universidad Austral de Chile (FOND-EQUIP EQM180042).

References

- Alcock, C., Allsman, R., Alves, D., et al. 2003, VizieR Online Data Catalog, II/247
 Alcock, C., Allsman, R., Alves, D. R., et al. 2000, The Astrophysical Journal, 542, 281

² <https://github.com/astromer-science>

- Alcock, C., Allsman, R., Alves, D. R., et al. 1999, Publications of the Astronomical Society of the Pacific, 111, 1539
- Becker, I., Pichara, K., Catelan, M., et al. 2020, Monthly Notices of the Royal Astronomical Society, 493, 2981
- Bishop, C. M. 1995, Neural computation, 7, 108
- Catelan, M. 2004, in International Astronomical Union Colloquium, Vol. 193, Cambridge University Press, 113–123
- Charnock, T. & Moss, A. 2017, The Astrophysical Journal Letters, 837, L28
- de Vries, W., van Cranenburgh, A., Bisazza, A., et al. 2019, arXiv preprint arXiv:1912.09582
- Devlin, J., Chang, M.-W., Lee, K., & Toutanova, K. 2018, arXiv preprint arXiv:1810.04805
- Dhar, P. 2020, Nature Machine Intelligence, 2, 423
- Donoso-Oliva, C., Cabrera-Vives, G., Protopapas, P., Carrasco-Davis, R., & Estevez, P. 2021, Monthly Notices of the Royal Astronomical Society
- Glorot, X. & Bengio, Y. 2010, in Proceedings of the thirteenth international conference on artificial intelligence and statistics, JMLR Workshop and Conference Proceedings, 249–256
- Heinze, A., Tonry, J. L., Denneau, L., et al. 2018, The Astronomical Journal, 156, 241
- Ivezić, Ž., Kahn, S. M., Tyson, J. A., et al. 2019, ApJ, 873, 111
- Jamal, S. & Bloom, J. S. 2020, The Astrophysical Journal Supplement Series, 250, 30
- Kingma, D. P. & Ba, J. 2014, arXiv preprint arXiv:1412.6980
- Kremer, J., Stensbo-Smidt, K., Gieseke, F., Pedersen, K. S., & Igel, C. 2017, IEEE Intelligent Systems, 32, 16
- LeCun, Y., Bengio, Y., & Hinton, G. 2015, nature, 521, 436
- Liu, X., Zhang, F., Hou, Z., et al. 2021, IEEE Transactions on Knowledge and Data Engineering
- Liu, Y., Ott, M., Goyal, N., et al. 2019, arXiv preprint arXiv:1907.11692
- Masala, M., Ruseti, S., & Dascalu, M. 2020, in Proceedings of the 28th International Conference on Computational Linguistics, 6626–6637
- Moradshahi, M., Palangi, H., Lam, M. S., Smolensky, P., & Gao, J. 2019, arXiv preprint arXiv:1910.12647
- Naul, B., Bloom, J. S., Pérez, F., & van der Walt, S. 2018, Nature Astronomy, 2, 151
- Polignano, M., Basile, P., De Gemmis, M., Semeraro, G., & Basile, V. 2019, in 6th Italian Conference on Computational Linguistics, CLiC-it 2019, Vol. 2481, CEUR, 1–6
- Sánchez-Sáez, P., Reyes, I., Valenzuela, C., et al. 2021, The Astronomical Journal, 161, 141
- Szymański, M., Udalski, A., Soszyński, I., et al. 2011, arXiv preprint arXiv:1107.4008
- Tonry, J., Denneau, L., Heinze, A., et al. 2018, Publications of the Astronomical Society of the Pacific, 130, 064505
- Tsang, B. T.-H. & Schultz, W. C. 2019, The Astrophysical Journal Letters, 877, L14
- Udalski, A. 2004, arXiv preprint astro-ph/0401123
- Udalski, A., Szymański, M., & Szymański, G. 2015, arXiv preprint arXiv:1504.05966
- Vaswani, A., Shazeer, N., Parmar, N., et al. 2017, in Advances in neural information processing systems, 5998–6008
- Vunikili, R., Supriya, H., Marica, V. G., & Farri, O. 2020, in IberLEF@SEPLN, 505–511